

Yangwei Liu¹

National Key Laboratory of Science and
Technology on Aero-Engine
Aero-Thermodynamics,
School of Energy and Power Engineering;
Collaborative Innovation Center of Advanced
Aero-Engine,
Beihang University,
No. 37 Xueyuan Road, Haidian District,
Beijing 100191, China
e-mail: liuyangwei@126.com

Yumeng Tang

National Key Laboratory of Science and
Technology on Aero-Engine
Aero-Thermodynamics,
School of Energy and Power Engineering,
Beihang University,
No. 37 Xueyuan Road, Haidian District,
Beijing 100191, China
e-mail: tang_yumeng@126.com

Ashley D. Scillitoe

CFD Laboratory, Department of Engineering,
University of Cambridge,
Cambridge CB2 1PZ, UK
e-mail: ascillitoe@turing.ac.uk

Paul G. Tucker

CFD Laboratory, Department of Engineering,
University of Cambridge,
Cambridge CB2 1PZ, UK
e-mail: pgt23@cam.ac.uk

Modification of Shear Stress Transport Turbulence Model Using Helicity for Predicting Corner Separation Flow in a Linear Compressor Cascade

Three-dimensional corner separation significantly affects compressor performance, but turbulence models struggle to predict it accurately. This paper assesses the capability of the original shear stress transport (SST) turbulence model to predict the corner separation in a linear highly loaded prescribed velocity distribution (PVD) compressor cascade. Modifications for streamline curvature, Menter's production limiter, and the Kato-Launder production term are examined. Comparisons with experimental data show that the original SST model and the SST model with different modifications can predict the corner flow well at an incidence angle of -7 deg, where the corner separation is small. However, all the models overpredict the extent of the flow separation when the corner separation is larger, at an incidence angle of 0 deg. The SST model is then modified using the helicity to take account of the energy backscatter, which previous studies have shown to be important in the corner separation regions of compressors. A Reynolds stress model (RSM) is also used for comparison. By comparing the numerical results with experiments and RSM results, it can be concluded that sensitizing the SST model to helicity can greatly improve the predictive accuracy for simulating the corner separation flow. The accuracy is quite competitive with the RSM, whereas in terms of computational cost and robustness it is superior to the RSM.
[DOI: 10.1115/1.4045658]

Keyword: computational fluid dynamics

1 Introduction

Three-dimensional corner separation, which is an inherent flow feature of the corner formed by the blade suction surface and endwall of axial compressors, may lead to deleterious consequences, for example, passage blockage, limitation of blade loading and static pressure rise, considerable total pressure loss, efficiency reduction and eventually stall or surge, especially in highly loaded compressors [1,2]. Hence, there is a need to effectively control corner separations during the design of axial compressors, which requires them to be accurately predicted by computational fluid dynamics (CFD) tools. During the last several decades, previous studies have been made on studying the flow mechanisms [3–6], prediction methods [7–10], and flow control techniques [11–15] of corner separations under various flow conditions.

With the rapid growth of computing power, the CFD technique has an increasingly significant role in the aerodynamic design of compressors [16]. The Reynolds-averaged Navier-Stokes equations (RANS) method is still the most widely used approach due to its small computational cost. But direct numerical simulation, large eddy simulation (LES), and hybrid LES/RANS have been utilized to investigate flow mechanisms at relatively low Reynolds number with simple boundary conditions [17–21]. The RANS

method remains in high demand for engineering and will be for over 50 years [22]. Errors of the RANS method as used for routine turbomachinery design can mainly arise from the assumption of steady flow [23] and turbulence models [24]. However, there is no single turbulence model that is universally superior for all kinds of flow problems. This is especially true for complex turbomachinery flows, where large regions of separated flow and vortical flow exist [18,25,26].

Most commonly used turbulence models are constructed using a number of assumptions, such as a local equilibrium between turbulence production and destruction, or the assumption that turbulence is isotropic. Many modifications have been proposed to improve turbulence models for application to specific flows [27,28]. In an axial compressor, significant streamline curvature is present, and the turbulence can be highly anisotropic, with a lack of equilibrium between production and dissipation. Scillitoe et al. [8] recently studied the capability of turbulence models to predict the corner separation flow physics in a linear compressor cascade. The one-equation SA model [29] and SA model with corrected streamline curvature [30], anisotropy [31], and non-equilibrium [32] effects were tested. Although certain corrections improved the performance in some areas, no correction showed a universal improvement, with all of them struggling in some areas. It was concluded that the one-equation SA model with the above corrections could not accurately account for the complex turbulence characteristics of corner separation in compressors. Thus, there is a need for further studies on turbulence modeling of corner separation flow.

The widely used shear stress transport (SST) model is a relatively robust and accurate two-equation eddy-viscosity turbulence model [33]. The SST model was introduced by Menter in 1994 [34].

¹Corresponding author.

Contributed by the Heat Transfer Division of ASME for publication in the JOURNAL OF TURBOMACHINERY. Manuscript received May 14, 2019; final manuscript received November 22, 2019; published online December 9, 2019. Assoc. Editor: Rakesh Srivastava.

It was originally designed to accurately predict aeronautics flows with strong adverse pressure gradients and separation but has since been used for a wide range of flows. However, recent studies indicate that the SST model with existing modifications for production limiters [8,10] cannot correctly predict the extent of the three-dimensional corner separation that occurs in compressors. A modified SST model [35], based on an adaptation of the rotation-curvature correction by Spalart and Shur [30], has been tested on a wide range of both wall-bounded and free shear turbulent flows. Significant improvements were achieved by the proposed corrections in terms of accuracy. Therefore, it is of interest to investigate whether the SST model with different corrections can accurately predict the corner separation.

In the corner separation, a number of multi-scale vortical flow structures are present, such as a horseshoe vortex, passage vortex, wake shedding vortex, and corner vortex [19]. Numerous studies have shown that strong turbulence energy backscatter exists in vortical flows, and there is a strong correlation between velocity helicity and turbulent energy backscatter [36–38]. Helicity, which is the streamwise vorticity of flow, was first proposed in relation to fluid flow by Moffatt in 1969 [39]. Though helicity is not Galilean invariant and it will be dependent on your frame of reference, it is of great significance for turbulence and it has been attracting great attention. It is a promising strategy to improve the turbulence model based on helicity to consider the energy backscatter, though this lack of Galilean invariance makes turbulence model less general. It is an inviscid invariance that is conserved in inviscid flows. Recently, two papers published in the journal Science also focused on the evolution of helicity. Scheeler et al. [40] experimentally studied the evolution of helicity in viscous fluids and concluded that helicity can remain constant even in a viscous fluid; Moffatt pointed out that it is vital to understand how helicity inhibits the energy cascade to the smallest scales, at which turbulent energy is dissipated as heat [41]. It follows that non-zero helicity should lead to a decrease in turbulent viscosity [42]. Recently, Liu et al. [7] made the first attempt to modify the turbulence model using helicity to consider the turbulence energy backscatter in vortical flows, and the strategy can significantly improve the SA turbulence model to predict complex flows, especially for massive separation flows in linear compressor cascades [7,43] and stall margin in several fans using steady or unsteady simulations [44,45]. This paper examines whether a similar strategy can be used to improve the SST model for the prediction of corner separations.

In this paper, the original SST model and SST model with existing modifications, including a streamline curvature correction, Menter's production limiter [33], and Kato-Launder production term [46], are examined numerically. The flow to be investigated is the corner separation in a highly loaded linear compressor cascade, studied experimentally by Gbadebo et al. [4,11]. The numerical results of the SST model with existing modifications are compared with the experimental data, and the capacities for predicting the three-dimensional corner separation flow are evaluated in detail. The original SST model and SST model with existing

Table 1 Geometrical parameters of PVD compressor cascade

| Parameter | Value | Parameter | Value |
|----------------|--------|---------------------|-------|
| Chord/ c (m) | 0.1515 | Inlet angle (deg) | 41 |
| Solidity | 1.08 | Chamber angle (deg) | 42 |
| Aspect ratio | 1.32 | Stagger angle (deg) | 14.7 |

modifications are all found to significantly overpredict the corner separation extent when the separation is large. Therefore, a new modification for the SST model based on helicity, similar to the study by Liu et al. [7], is proposed. By comparing the numerical results with experiments and Reynolds stress model (RSM) results, the modification for the SST model based on helicity is validated in detail.

2 Computational Setup

2.1 Computational Domain. The investigated geometry is a linear prescribed velocity distribution (PVD) cascade made up of highly loaded controlled diffusion aerofoils. It was investigated experimentally by Gbadebo et al. [4,11]. The cascade geometrical parameters are listed in Table 1.

A single cascade passage is adopted as the computational domain with its inlet located $2c$ (chord) upstream of the blade leading edge, to match the incoming flow measurement position in the experiment. The outlet of the computational domain is set $2c$ downstream the trailing edge with a buffer zone to avoid spurious waves. Accounting for the symmetry of the linear cascade passage, only half of the span is considered. A translational periodic boundary condition is used in the pitch-wise direction, to satisfy the infinite blade count assumption. The whole computational domain and the measurement plane location are shown in Fig. 1.

A structured multi-block O4H mesh is generated using Auto-Grid5TM, with the near-wall mesh resolution set to ensure $y^+ < 1$. A series of meshes are generated with different densities and distributions to check the grid independence of the solution. The total grid number of 0.98×10^6 , 1.56×10^6 , 1.85×10^6 , and 2.37×10^6 have been examined. Flow details, including static pressure coefficient, the total pressure loss coefficient, the relative displacement thickness, and the exit flow angle, have been compared to confirm the grid independence. Grid independence is achieved with a mesh consisting of 1.56×10^6 mesh points, with 81 nodes distributed in the spanwise direction. This mesh is used for all subsequent computations.

2.2 Numerical Scheme and Boundary Conditions. The inlet Mach number is approximately 0.07. Hence, the pressure-based solver which is more suitable for incompressible or low Mach flow is used for all simulations, and pressure-velocity coupling is handled by the SIMPLE algorithm. A second-order accurate

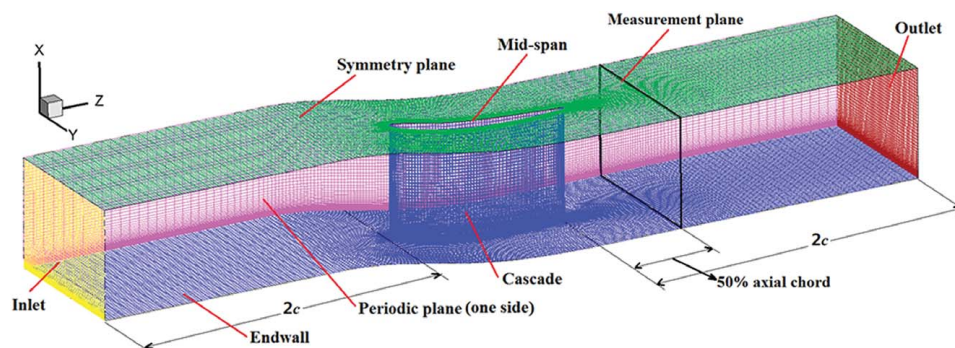


Fig. 1 Computational domain of PVD linear cascade

upwind scheme [47] is used for the convective terms, while second-order central-differencing is used for the diffusive terms.

In all the simulations, the inlet velocity profile and outlet static pressure are set to be consistent with the experimental measurements [48], to make a fair comparison with the experiments. The inlet turbulent intensity is set at 1.5%, in order to match that measured one in the experiment. The endwall and blade surface are set as non-slip walls. To reduce the computation cost, only half of the cascade blade span is meshed, with a symmetry plane enforced at the blade mid-span.

The cascade was tested experimentally under two incidences, namely 0 deg and -7 deg, of which the former is the design point. The corner separation is noticeably larger at an incidence angle of 0 deg, compared with that at an incidence angle of -7 deg. Therefore, in this paper, the 0 deg case is referred to as the large separation condition case, and the -7 deg case is referred to as the small separation condition case.

2.3 The Shear Stress Transport Model With Different Existing Modification. This section introduces the original SST model proposed by Menter [34], and several existing modifications made to it.

2.3.1 The Shear Stress Transport Turbulence Model. Most of the commonly used turbulence models except the RSM are based on the Boussinesq hypothesis, which defines the Reynolds stress tensor as:

$$-\rho \overline{u_i' u_j'} = \mu_t \left(2S_{ij} - \frac{2}{3} \delta_{ij} \frac{\partial u_k}{\partial x_k} \right) - \frac{2}{3} \delta_{ij} \rho k \quad (1)$$

where $-\rho \overline{u_i' u_j'}$ represents the Reynolds stress, μ_t is the turbulent viscosity, δ_{ij} is Kronecker delta function assigning $\delta_{ij} = 1$ if $i = j$ and $\delta_{ij} = 0$ if $i \neq j$, and k is the turbulence kinetic energy. S_{ij} represents the mean strain-rate tensor, given by

$$S_{ij} = \frac{1}{2} \left(\frac{\partial u_i}{\partial x_j} + \frac{\partial u_j}{\partial x_i} \right) \quad (2)$$

The SST turbulence model was used to close the RANS equations in the current study. This model solves additional transport equations for the turbulence kinetic energy k , and the specific dissipation of turbulence ω

$$\frac{\partial}{\partial t} (\rho k) + \frac{\partial}{\partial x_i} (\rho k u_i) = \frac{\partial}{\partial x_j} \left(\Gamma_k \frac{\partial k}{\partial x_j} \right) + P_k - Y_k \quad (3)$$

$$\frac{\partial}{\partial t} (\rho \omega) + \frac{\partial}{\partial x_j} (\rho \omega u_j) = \frac{\partial}{\partial x_j} \left(\Gamma_\omega \frac{\partial \omega}{\partial x_j} \right) + P_\omega - Y_\omega + D_\omega \quad (4)$$

In the above equations, Γ_k and Γ_ω represents the effective diffusivity of k and ω , respectively. The terms P_k , P_ω , Y_k , and Y_ω represent the production of turbulence kinetic energy k , the production of ω , the dissipation of turbulence kinetic energy k and the dissipation of ω , respectively. The term D_ω is a cross-diffusion term, which is introduced to better blend the $k-\varepsilon$ and $k-\omega$ models together, to form the SST model. More details about these terms can be seen in Ref. [34].

The term P_k is defined as

$$P_k = -\rho \overline{u_i' u_j'} \frac{\partial u_j}{\partial x_i} \quad (5)$$

The term P_ω is defined as

$$P_\omega = \alpha \frac{\rho}{\mu_t} P_k \quad (6)$$

where α is a model coefficient.

Based on the Boussinesq hypothesis, P_k is modeled as

$$P_k = \mu_t S^2 \quad (7)$$

where S is the modulus of the mean rate-of-strain tensor, defined as

$$S \equiv \sqrt{2S_{ij}S_{ij}} \quad (8)$$

The key feature of the SST turbulence model lays in its definition of the turbulent viscosity, which considers the transport of turbulent shear stress in order to limit overprediction of the turbulent viscosity

$$\mu_t = \frac{\rho a_1 k}{\max[a_1 \omega, SF_2]} \quad (9)$$

where S is the strain-rate magnitude given in Eq. (8), and $a_1 = 0.31$. The blending function F_2 is given by

$$F_2 = \tanh \left(\max \left[2 \frac{\sqrt{k}}{0.09 \omega y}, \frac{500 \mu}{\rho y^2 \omega} \right] \right)^2 \quad (10)$$

where y is the distance to the nearest wall.

2.3.2 Existing Modifications for Shear Stress Transport Model. One drawback of the linear eddy-viscosity models, such as the SST model, is their insensitivity to streamline curvature and system rotation, which are commonly seen in many turbulent flows of practical interest. Smirnov and Menter [35] propose an efficient approach to sensitize the standard two-equation turbulence models to streamline curvature and system rotation. The approach builds upon Spalart and Shur's [30] correction, which sensitizes the SA model to curvature and rotation through a rotation function defined as

$$f_{rotation} = (1 + c_{r1}) \frac{2r^*}{1 + r^*} [1 - c_{r3} \tan^{-1}(c_{r2} \tilde{r})] - c_{r1} \quad (11)$$

where the empirical constants c_{r1} , c_{r2} , and c_{r3} are set to 1.0, 2.0, and 1.0, respectively. The arguments r^* and \tilde{r} are defined as follows:

$$r^* = \frac{S}{\Omega} \quad (12)$$

$$\tilde{r} = 2\Omega_{ik} S_{ik} \left[\frac{DS_{ij}}{Dt} + (\varepsilon_{imn} S_{jn} + \varepsilon_{jmn} S_{im}) \Omega_m^{Rot} \right] \frac{1}{\tilde{D}} \quad (13)$$

where DS_{ij}/Dt are the components of the Lagrangian derivative of the strain-rate tensor. The modulus of the mean rate-of-strain tensor S is given in Eq. (8), and the vorticity tensor and its modulus are defined as follows:

$$\Omega_{ij} = \frac{1}{2} \left(\frac{\partial u_i}{\partial x_j} - \frac{\partial u_j}{\partial x_i} \right) + 2\varepsilon_{mji} \Omega_m^{rot} \quad (14)$$

$$\Omega \equiv \sqrt{2\Omega_{ij}\Omega_{ij}} \quad (15)$$

For two-equation models, Smirnov and Menter [35] rewrite the denominator in Eq. (13) to have the following form:

$$\tilde{D} = \Omega D^3 \quad (16)$$

$$D^2 = \max(S^2, 0.09\omega^2) \quad (17)$$

The SST model with curvature correction (abbreviated CC in this paper) is obtained by multiplying the function f_{r1} by the production term P_k

$$\tilde{P}_k = P_k f_{r1} \quad (18)$$

with

$$f_{r1} = \max\{\min(f_{rotation}, 1.25), 0\} \quad (19)$$

Another disadvantage of the widely used two-equation turbulence models is the excessive production of the turbulence kinetic energy P_k in the vicinity of stagnation points. The complete

formulation of the SST model proposed by Menter (1994) [34] limits P_k

$$\tilde{P}_k = \min(P_k, C_{lim}\rho\epsilon) \quad (20)$$

where the coefficient C_{lim} is set to 10 by default. This limiter makes no difference to the shear layer performance of the model, but avoids unphysical turbulent energy buildup in stagnation regions. The above modification method is called Menter's production limiter (abbreviated PL in this paper).

Kato and Launder (1993) [46] noticed that the excessive level of turbulence kinetic energy production is caused by the very high level of shear strain rate in the stagnation regions. The flow field near a stagnation point is nearly irrotational, with a very small vorticity rate Ω . Therefore, they presented an approach to modify the formula for the turbulence kinetic energy production term P_k , given in Eq. (7), to:

$$\tilde{P}_k = \mu_r S \Omega \quad (21)$$

where S and Ω are the modulus of the mean rate-of-strain tensor and the vorticity tensor given in Eqs. (8) and (15), respectively. This modification method is called the Kato-Launder production term (abbreviated KL in this paper).

The SST model modifications mentioned above are investigated in this paper, and the numerous combinations used are summarized in Table 2.

2.4 The Reynolds Stress Model. The RSM abandons the isotropic eddy-viscosity hypothesis and closes the RANS equations by solving transport equations for Reynolds stresses together with an equation for the dissipation rate [49]. Adding seven equations for three-dimensional resolution. The RSM accounts for more complex flow effects such as streamline curvature, swirl, rotation and rapid changes in the strain rate in a more rigorous way with an exact representation of the Reynolds stress than the classical two-equation eddy-viscosity models, though the RSM suffers issues in terms of the robustness and computational cost in engineering application.

3 Assessment of Shear Stress Transport Model With Existing Modifications

3.1 Definition of Flow Field Parameters. A number of parameters are used to study the flow field in the cascade. The static pressure coefficient C_p is defined as

$$C_p = \frac{p - p_1}{\frac{1}{2}\rho U_1^2} \quad (22)$$

And the total pressure loss coefficient Y_p is defined as

$$Y_p = \frac{p_{01} - p_0}{\frac{1}{2}\rho U_1^2} \quad (23)$$

where p_{01} is the inlet total pressure, p_1 is the inlet static pressure, and U_1 is the bulk velocity of the incoming flow. Similarly, p_0 is the

local total pressure and p is the local static pressure. The fluid density ρ is held constant at 1.225 kg/m^3 .

The concept of relative displacement thickness, introduced by Gbadebo [11], is used to evaluate the effects of three-dimensional separation on blockage, namely the thickness of the three-dimensional separated region over the suction surface. It is expressed as the displacement thickness at any span position minus the mid-span one. Since the flow usually does not separate at the mid-span except complete blade stall, the net or relative displacement thickness at those radial locations would be equivalent to the contribution from the separated boundary layer. At each span position, the displacement thickness can be obtained by

$$\delta^*(x) = \int_0^\delta \left[1 - \frac{\rho v(x, y)}{\rho_{fs} V_{fs}} \right] dy \quad (24)$$

where x is the spanwise location, y is the distance from the suction surface, v is the velocity, and the subscript fs is for the local free-stream. The so-called relative displacement thickness can be expressed as

$$\delta_{eff}^* = \frac{\delta^*(x) - \delta_{mid}^*}{c} \quad (25)$$

3.2 Flow Field Analysis of Shear Stress Transport Model With Existing Modifications

3.2.1 Incidence Angle of -7 deg. The surface static pressure coefficient is an important quantity, closely linked to the aerodynamic performance of the cascade. It determines the pressure gradient and the diffusion level, which contribute to the three-dimensional corner separation. Figure 2 plots the static pressure coefficient C_p against the normalized axial location x/C_x for the -7 deg incidence angle case. Distributions are shown at two spanwise locations, 89% span (11% from the endwall) and 54% span (4% span from the mid-span). Comparisons are made between experimental measurements and simulating results from SST model with all the modifications listed in Table 2.

The corner separation extent under the incidence angle of -7 deg is small. In this case, the SST model and all the modifications tested are seen to agree relatively well with the experimental results. Discrepancies between different corrections are minimal.

Figure 3 shows the measured and simulated total pressure loss coefficient contours at 50% axial chord downstream of the trailing edge under the incidence angle of -7 deg. The original SST model and its existing modifications (not shown here due to paper length) predict the corner separation nearly the same. The loss core due to the corner separation at the blade-endwall junction, as well as losses due to the blade wake, is visible. The losses predicted by the SST models are slightly higher than the experimental measurements in the high loss core region and the wake center. However, the extent of the high loss in the separated region is predicted moderately well by all the models. This suggests the original SST model, and its existing modifications can all reliably predict the corner separation under the small separation condition.

Table 2 Different modifications investigated in this work

| Turbulence model | Modification methods | Abbr. |
|------------------|--|------------|
| SST [34] | None | SST |
| | Curvature correction (CC) [30] | SST_CC |
| | Menter's production limiter (PL) [34] | SST_PL |
| | Kato-Launder production term (KL) [46] | SST_KL |
| | Menter's Production Limiter & Curvature Correction (PLCC) | SST_PLCC |
| | Menter's Production Limiter & Kato-Launder Production Term (PLKL) | SST_PLKL |
| | Kato-Launder Production Term & Curvature Correction (KLCC) | SST_KLCC |
| | Menter's Production Limiter & Kato-Launder Production Term & Curvature Correction (PLKLCC) | SST_PLKLCC |

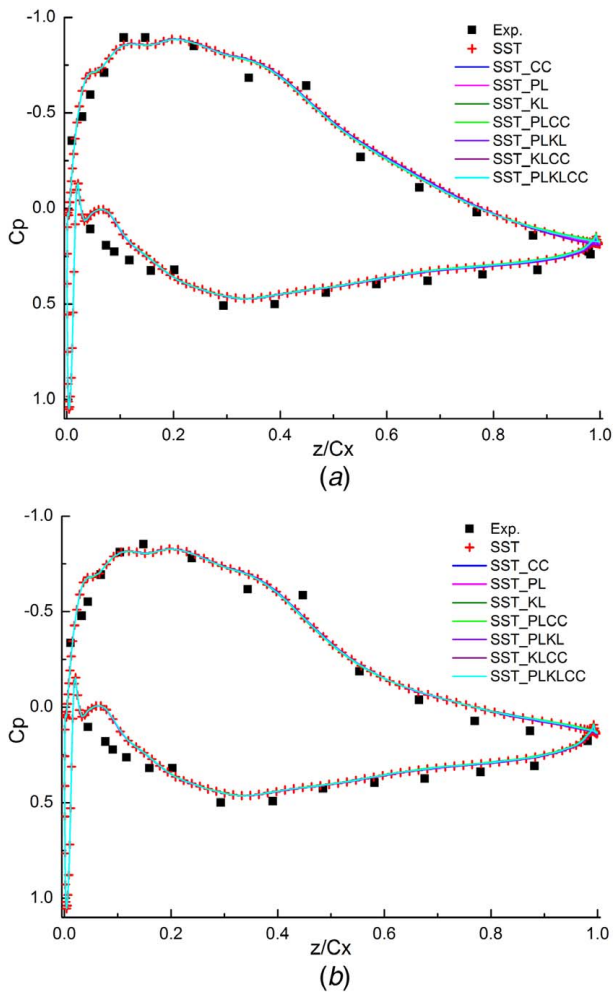


Fig. 2 Surface static pressure coefficient at different span locations under the incidence angle of -7 deg by SST model with different modifications: (a) 54% span and (b) 89% span

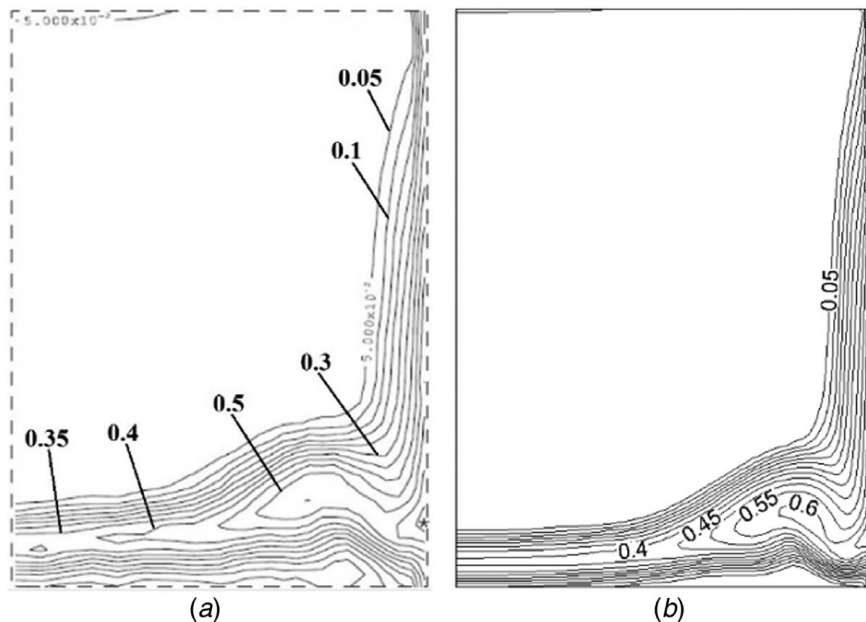


Fig. 3 Total pressure loss coefficient contours at 50% axial chord downstream of the trailing edge, at an incidence angle of -7 deg by SST model: (a) experimental measurement and (b) SST model

3.2.2 Incidence Angle of 0 deg. Results from the original SST model and SST model with modifications for the 0 deg incidence angle case are presented in Figs. 4–7. The SST model over predicts the corner separation extent, with premature separation on the blade suction surface. This is especially apparent in the C_p distribution close to the endwall, shown in Fig. 4(b). None of the modifications are seen to help here, with all the corrections giving similar predictions to the original SST model.

Figure 5 presents the total pressure loss coefficient at 50% axial chord downstream of the trailing edge. The SST model (and modifications) all overpredict the magnitude of loss in the high loss core region, with loss coefficients of up to $Y_p = 0.75$, compared to $Y_p = 0.55$ measured in the experiment. Compared to the original SST model, the PL modification's influence is negligible; the KL modification predicts a slightly smaller corner separation and less wake loss, whereas the CC modification predicts a slightly larger corner separation and greater wake loss.

To analyze the above differences quantitatively, the total pressure loss coefficient and exit flow angle are pitch-wise averaged at the measurement plane shown in Fig. 1. The spanwise distributions of these quantities are shown in Fig. 6. Large discrepancies can be found between numerical results and experiment results. The total pressure loss coefficient and deviation angle are significantly overpredicted across most of the span, which is consistent with Fig. 5.

Furthermore, the relative displacement thickness distributions across the trailing edge are plotted in Fig. 7. The pitch-wise and spanwise extents of the corner separation are significantly overpredicted by the SST model and all the modifications tested. Differences between the modifications are more obvious here than in the total pressure loss coefficient and exit flow angle predictions; however, they are still small.

4 Modification of Shear Stress Transport Model Using Helicity

4.1 Modified Shear Stress Transport Turbulence Model.

As discussed previously, helicity can represent the energy backscatter in vortical flows [36,37,38]. Liu et al. [7] use helicity in an attempt to add turbulent energy backscatter behavior to the SA

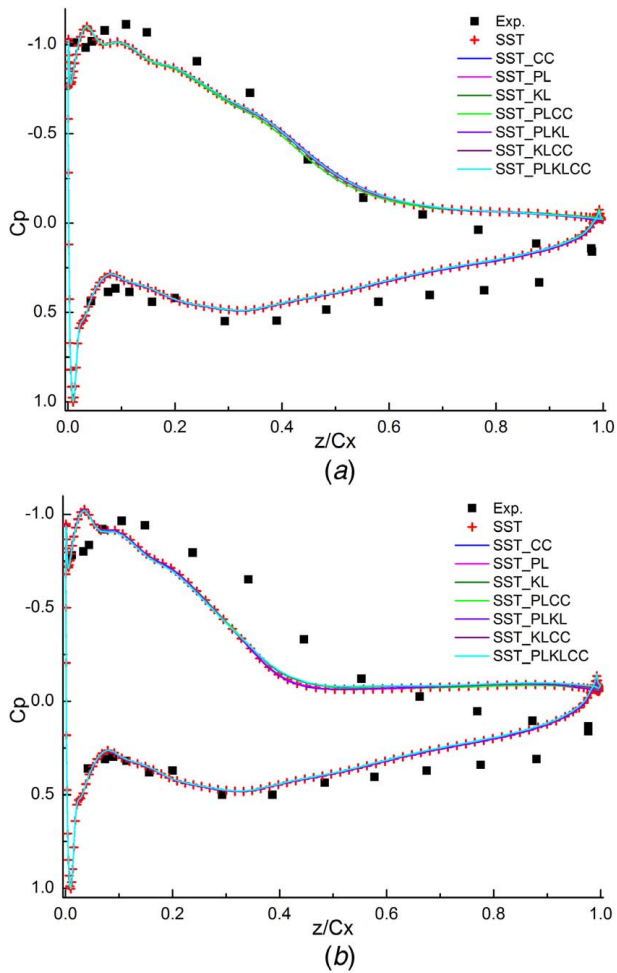


Fig. 4 Surface static pressure coefficient at different span locations at incidence angle of 0 deg by SST model with different modifications: (a) 54% span and (b) 89% span

model (named SA-helicity). The results show that the modified SA-helicity model significantly improves the predictive accuracy for simulating the corner separation flow in compressors. The numerical results show that the SA model and the SST model show similar performance for predicting the corner separation. They both significantly overpredict the corner separation when the separation is large. This is mainly because the turbulence is strongly non-equilibrium in massive separation flow and vertical flow, such as corner separation. Hence, a similar modification is now proposed to modify the original SST turbulence model (named SST-helicity in this paper).

The original production term P_k in both the SST equations is replaced by a new production term P_{kh} , which takes the following form:

$$P_{kh} = \mu_t f_{rh}(h) \Omega^2 = \mu_t (1 + C_{h1} h^{C_{h2}}) \Omega^2 \quad (26)$$

where h is the absolute value of relative helicity density, defined as

$$h = \left| \frac{\mathbf{v} \cdot \boldsymbol{\omega}}{|\mathbf{v}| |\boldsymbol{\omega}|} \right| \quad (27)$$

\mathbf{v} is the velocity vector and $\boldsymbol{\omega}$ is the vorticity vector. The two constants C_{h1} and C_{h2} are kept the same as the SA-helicity model [7], with $C_{h1} = 0.71$ and $C_{h2} = 0.6$, respectively. Here, Ω^2 instead of S^2 is used to make it consistent with the modification of SA-helicity model [7], though Ω^2 and S^2 could give similar results for predicting corner separation. The newly induced self-adaptive function

$f_{rh}(h) = 1 + C_{h1} h^{C_{h2}}$, that associates the production term P_{kh} with h , is plotted in Fig. 8. It can be seen from Eq. (27) that h ranges in a closed interval from 0 to 1. It has been found that a joint cascade of energy and helicity exists for the decay of 3D turbulence [50]. The function $f_{rh}(h)$ is positively correlated with h , so that the production term P_{kh} is amplified in regions with strong helicity if Ω^2 remains the same. This effect can be ignored in simple basic flows, whereas it cannot be neglected in vortically dominated 3D flows, such as the corner separation flow.

4.2 Assessment of the Modified Shear Stress Transport Turbulence Model. The newly introduced SST-helicity model is now used to predict the PVD cascade flow at the same two incidence angles as before. The CPU cost of the SST-helicity model is almost the same as original SST model, and the convergence of the SST-helicity model is better. This is mainly because the corner separation predicted by the original SST model is much larger. Usually predicting flow with smaller separation needs less iterations, and the residual is smaller.

4.2.1 Incidence Angle of 0 deg. Figure 9 shows the limiting streamlines on the endwall at 0 deg incidence angle, from the experiment, the original SST model result, and the SST-helicity result. The SST model predicts the endwall crossflow to roll up behind the suction leg of the horseshoe vortex, resulting in a bulk separation, or corner stall, which usually only occurs under high incidence angles. On the contrary, the SST-helicity model predicts an endwall flow in a much closer agreement with the experiment, with the endwall separation line located near the suction surface.

Figure 10 plots the surface static pressure distribution at 54% and 89% span locations. At both span locations, the C_p distribution predicted by the SST-helicity model is in better agreement with the measurements compared to the original SST model. Figure 9(b) shows the SST-helicity model provides a more reliable prediction for the onset of the corner separation. Consequently, the pressure recovery at both span locations is in closer agreement with the experiment.

As shown in Fig. 11, the helicity correction also significantly improves the downstream loss predictions. The loss coefficient in the high loss core is no longer over predicted, with $Y_p = 0.55$ predicted by the SST-helicity model, which is in agreement with the experimental measurements. The shear layer thickness simulated by the SST-helicity model is thicker than that simulated by the original SST model and agrees much better with the experimental measurements. Additionally, the SST-helicity model also predicts the loss in the wake center more accurately, with $Y_p = 0.4$. This is compared to the experimentally measured value of $Y_p = 0.4$, and the SST model value of $Y_p = 0.55$.

The spanwise distribution of pitch-wise averaged total pressure loss coefficient and exit flow angle at the measurement plane are plotted in Fig. 12, and the relative displacement thickness across the trailing edge is shown in Fig. 13. The SST-helicity model is also found to perform well here, with major improvements over the original SST model's predictions. Furthermore, the modified SST-helicity model has also been used to study corner separation control using blade end slots in a high-speed high-loading compressor cascade [51]. The results have been compared to validate numerical methods, and the comparison showed that the modified SST-helicity model predicts the separation very well.

4.2.2 Incidence Angle of -7 deg. In the above section, the results show that the SST-helicity model significantly improves the predictive accuracy of the corner separation at an incidence angle of 0 deg. In this section, the performance of the SST-helicity model for predicting the smaller separation condition, which the original SST predicted well, is examined. For brevity, only a selection of the key results are presented here.

The C_p distributions in Fig. 14 show that the helicity correction makes little difference to the aerodynamic performance of the

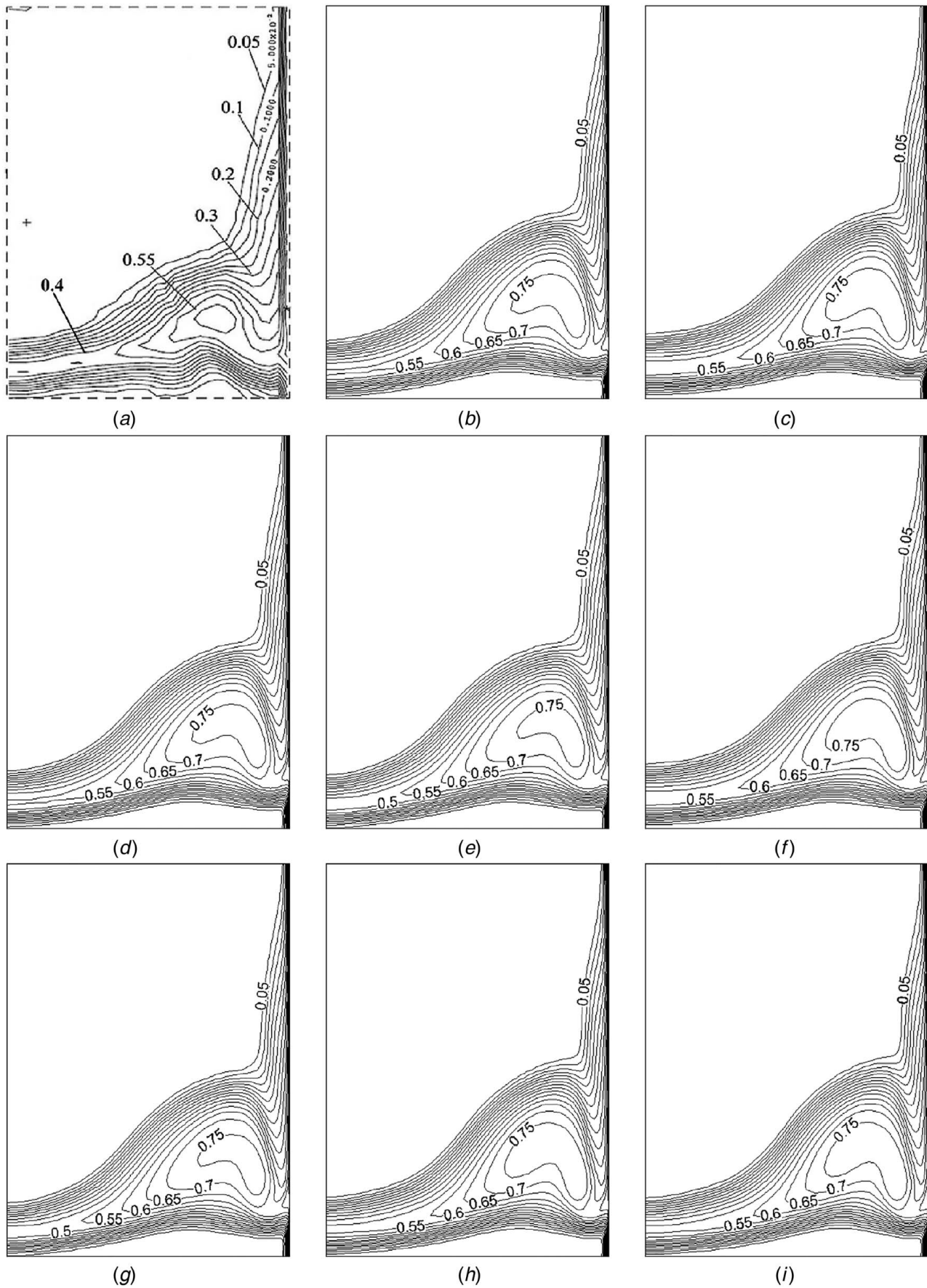


Fig. 5 Total pressure loss coefficient contours at 50% axial chord downstream of the trailing edge, at an incidence angle of 0 deg by SST model with different modifications: (a) experimental measurement, (b) SST, (c) SST_CC, (d) SST_PL, (e) SST_KL, (f) SST_PLCC, (g) SST_PLKL, (h) SST_KLCC, and (i) SST_PLKLCC

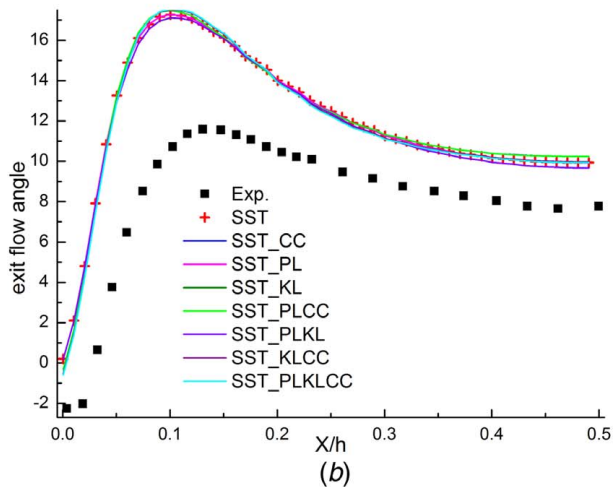
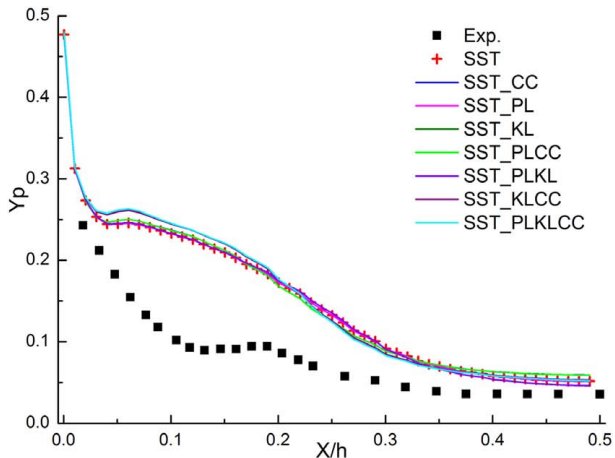


Fig. 6 Spanwise distribution of pitch-wise averaged parameters at 50% axial chord downstream of the trailing edge, at an incidence angle of 0 deg. Results for the SST model with different modifications: (a) total pressure loss coefficient and (b) exit flow angle.

cascade at this incidence. Only a small improvement in predictions is noticed toward the trailing edge.

Figure 15 presents the total pressure loss coefficient contour lines. Both the original and modified SST model mostly agree well with experimental measurements here, with just a slight

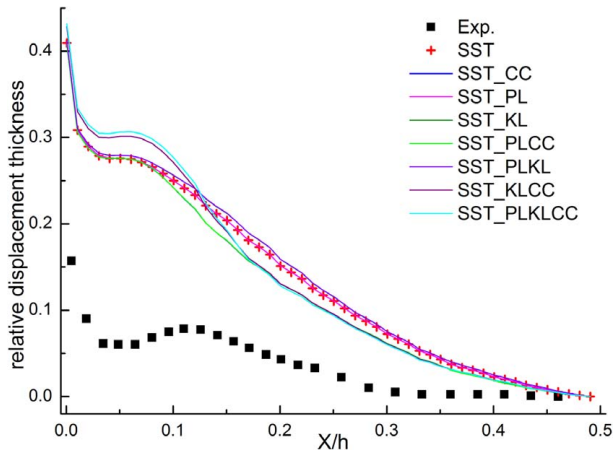


Fig. 7 Relative displacement thickness across the trailing edge at an incidence angle of 0 deg by SST model with different modifications

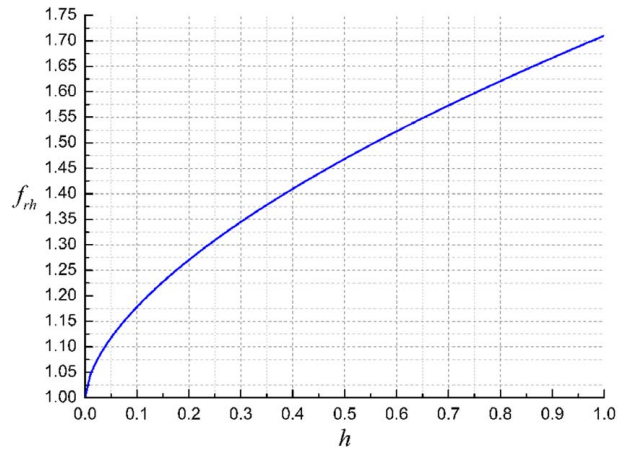


Fig. 8 Function of $f_{rh}(h)$

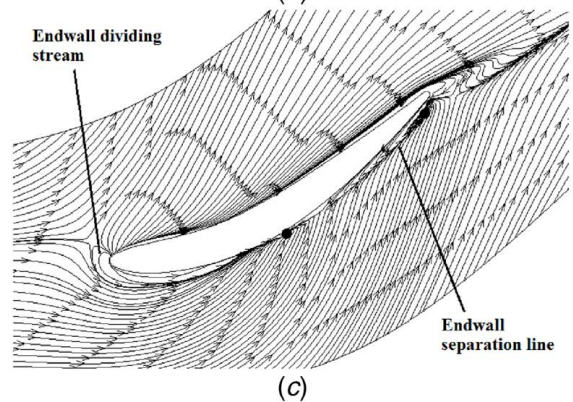
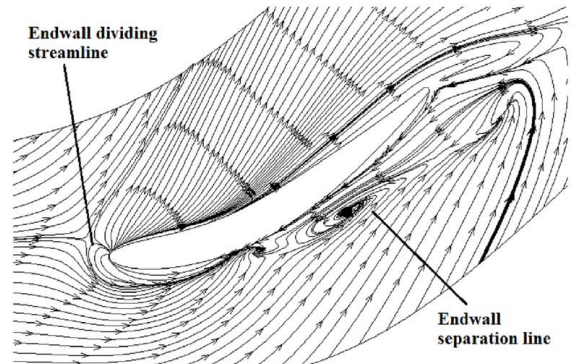
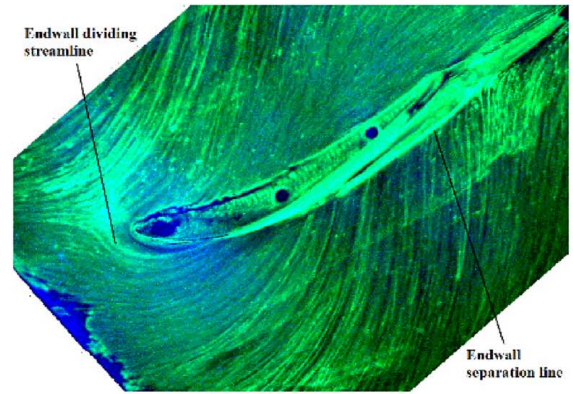


Fig. 9 Limiting streamlines on the endwall at an incidence angle of 0 deg by SST model and SST-helicity model: (a) experimental measurement, (b) original SST model, and (c) SST-helicity model

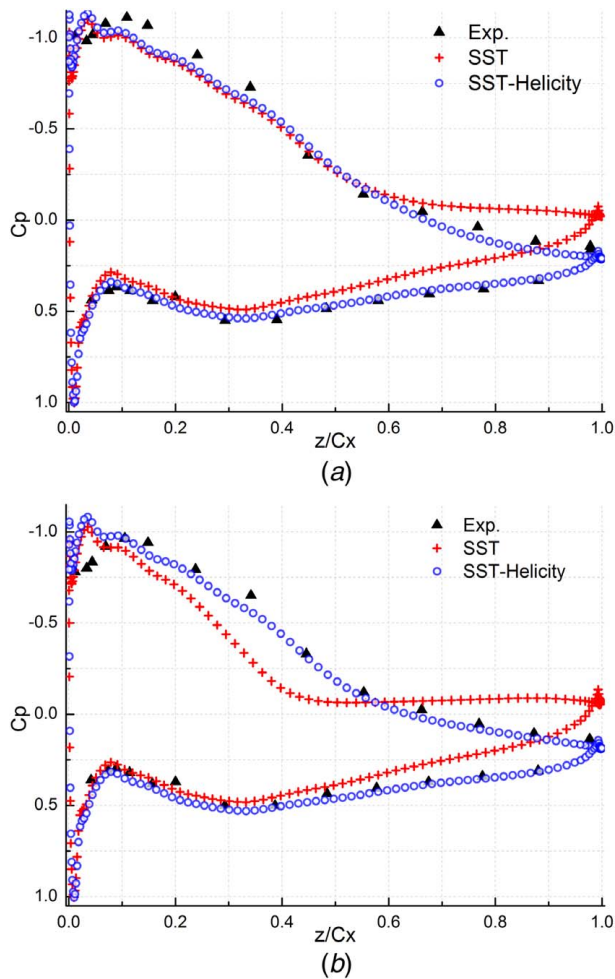


Fig. 10 Comparison of the surface static pressure coefficient at different span locations at an incidence angle of 0 deg by SST model and SST-helicity model: (a) 54% span and (b) 89% span

overprediction of loss inside the loss cores. The overprediction is less significant in the SST-helicity case, with a maximum loss of $Y_p = 0.55$ in the loss core region. This is compared with a measured maximum of $Y_p = 0.5$ in the experiment, and $Y_p = 0.6$ predicted by the SST model. Overall, the SST-helicity model shows slight improvements at this incidence angle. However, the original SST model already performed well at this incidence angle.

The above validations indicate that the proposed modification for the SST model based on helicity significantly improves the predictive accuracy for the three-dimensional corner separation in compressors.

4.3 Discussion. Figure 16 shows the turbulent viscosity at 50% axial chord downstream of the trailing edge. Note that the contour intervals for Figs. 16(a) and 16(b) are different because of the difference in the turbulent viscosity range returned by the two models. The helicity modification is seen to reduce the turbulent viscosity in the high loss core region, with about 50% less turbulent viscosity here compared to the original SST model result. These observations are in agreement with the differences in the total pressure loss predictions shown in Fig. 11. As shown in Fig. 8, the production term P_{kh} is amplified in regions with strong helicity if Ω^2 remains the same. Then, the predicted turbulent viscosity is decreased due to the nonlinear effect (as shown in Fig. 16).

The new function introduced in Sec. 4.1, $f_{rh}(h) = 1 + C_{h1}h^{C_{h2}}$, functions as a multiplier to the production term P_k . It increases smoothly according to the absolute value of relative helicity

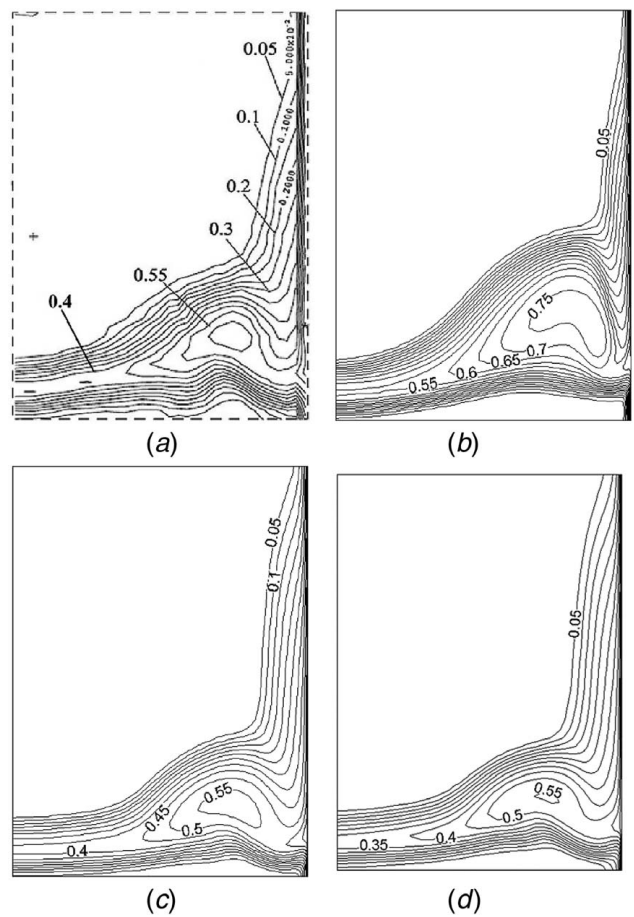


Fig. 11 Comparison of the total pressure loss coefficient at 50% axial chord downstream at an incidence angle of 0 deg by SST model and SST-helicity model: (a) experimental measurement, (b) SST result, (c) SST-helicity result, and (d) RSM_LPS result

density. As the absolute value of relative helicity density approaches zero, the multiplier approaches one, and hence the production term converges to $\mu_r\Omega^2$. To verify that the helicity modification remains passive outside of the corner separation region, the spanwise distributions of $f_{rh}(h)\Omega^2$, S^2 , and Ω^2 , 50% C_x upstream of the leading edge are plotted in Fig. 17. As expected, the magnitude of strain and vorticity are very similar in the attached turbulent boundary layer. Additionally, the helicity modification is seen to remain passive, since there is zero helicity in this region.

The helicity modification affects both the production and dissipation of turbulence. Therefore, the distributions of both are now examined further. However, there are no experimental measurements of these quantities available. Previous studies by Liu et al. [9,10] indicated that the more complex RSM with a linear pressure-strain model could predict the corner separation in the PVD cascade well. Hence, the RSM_LPS is now used for additional comparisons. As shown in Figs. 11 and 12, the RSM can generally predict the corner separation well, although it slightly underpredicts the corner separation extent. Comparing the RSM's results with the SST-helicity model's results in Figs. 11 and 12, it is apparent that the SST-helicity model is in closer agreement with the experimental measurements. This is especially the case in the spanwise flow angle distribution, where the RSM underpredicts the turning slightly. In terms of the robustness and computational cost, the SST-helicity is superior to the RSM.

Figures 18 and 19 show the non-dimensional production of turbulent kinetic energy P_k (or P_{kh} in the SST-helicity model) and turbulence dissipation rate $\rho\varepsilon$ at different streamwise sections, for the 0 deg incidence angle case. The incoming flow bulk velocity and

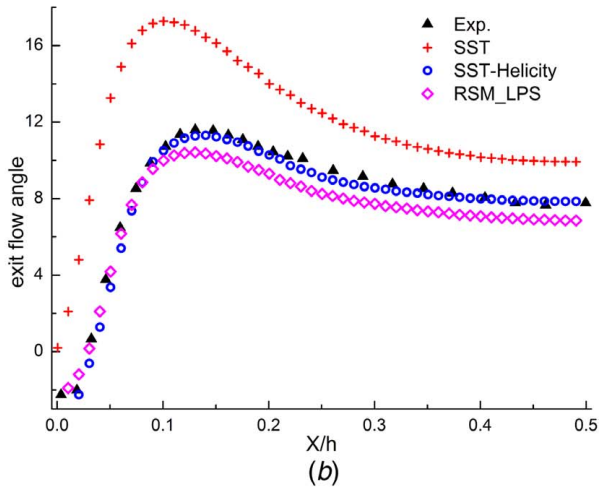
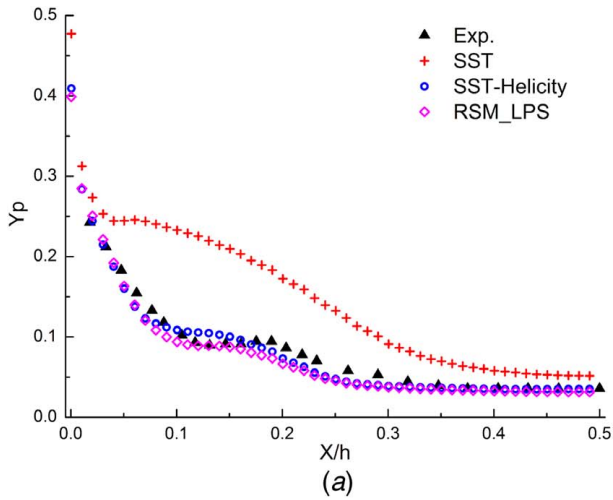


Fig. 12 Spanwise distribution of pitch-wise averaged parameters at 50% axial chord downstream of the trailing edge, at an incidence angle of 0 deg by SST model, SST-helicity model and RSM: (a) total pressure loss coefficient and (b) exit flow angle

chord length are used to non-dimensionalize the P_k (or P_{kh}) and $\rho\varepsilon$. Figures 18 and 19 show that the production of turbulent kinetic energy and turbulence dissipation rate $\rho\varepsilon$ predicted by the SST-helicity model are in significantly closer agreement with the RSM predictions, compared with those of the original SST model.

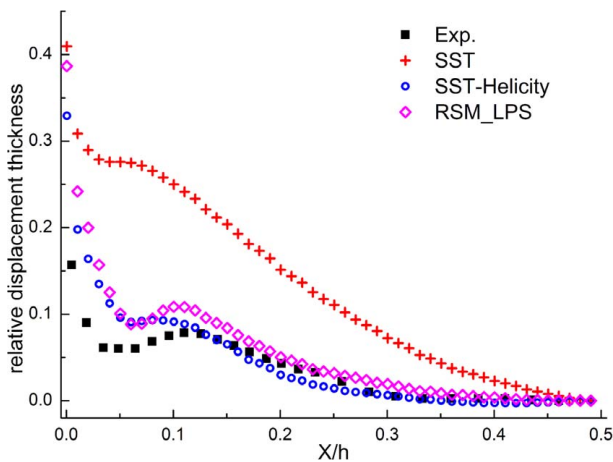


Fig. 13 Comparison of the relative displacement thickness across the trailing edge, at an incidence angle of 0 deg by SST model, SST-helicity model, and RSM

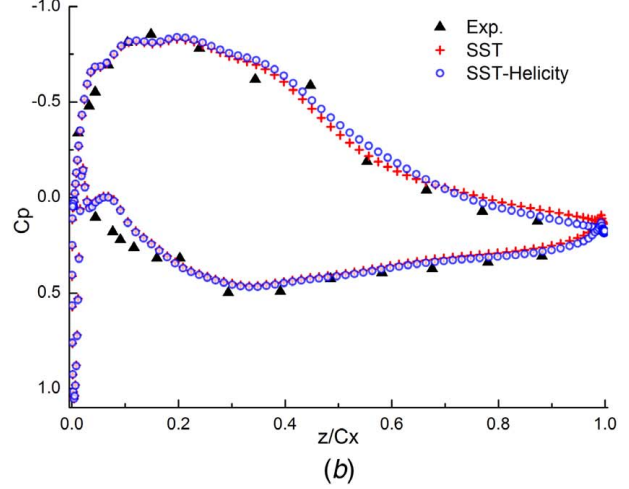
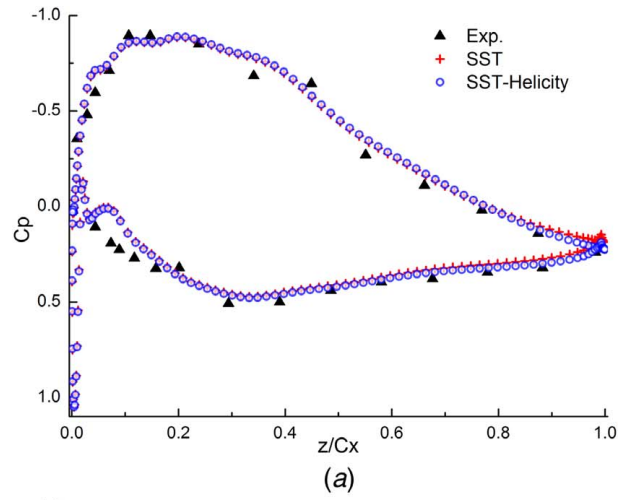


Fig. 14 Comparison of the surface static pressure coefficient at different span locations at an incidence angle of -7 deg by SST model and SST-helicity model: (a) 54% span and (b) 89% span

Figure 20 compares the ratio of production of turbulent kinetic energy (P_k or P_{kh}) to $\rho\varepsilon$ at 20% axial chord length downstream of the trailing edge. The black line features the regions where the production of turbulent kinetic energy P_k (or P_{kh}) is equal to the turbulence dissipation rate $\rho\varepsilon$, which can be regarded as being in a local state of equilibrium. Where separation occurs, the equilibrium state can be destroyed. The comparison in Fig. 20 shows that the original SST model overestimates the degree of non-equilibrium, whereas the SST-helicity is in close agreement with the RSM prediction.

5 Conclusions

The flow in the PVD linear cascade passage has been analyzed numerically using the SST model with a range of existing modifications, under two incoming flow conditions. The modifications studied include the streamline CC, PL, Kato-Launder production term (KL), and combinations of these. At a negative incidence angle, where the corner separation is small, all the models tested were in close agreement with experimental measurements. However, the original SST model, and all the existing modifications, overestimated the corner separation extent at an incidence angle of 0 deg. The origin of the corner separation on the suction surface occurs too far upstream, and a premature corner stall led to overpredictions in the total pressure loss.

The SST model is then modified using the helicity to take into account of turbulent energy backscatter, which is significant in

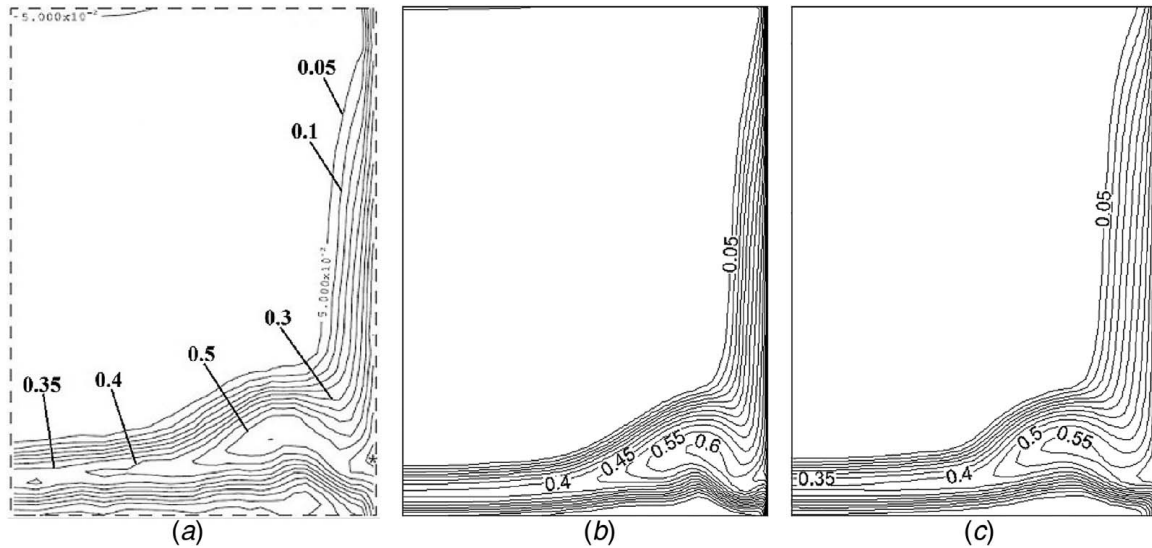


Fig. 15 Total pressure loss coefficient at 50% axial chord downstream of the trailing edge, at an incidence angle of -7 deg: (a) experimental measurement, (b) SST, and (c) SST-helicity

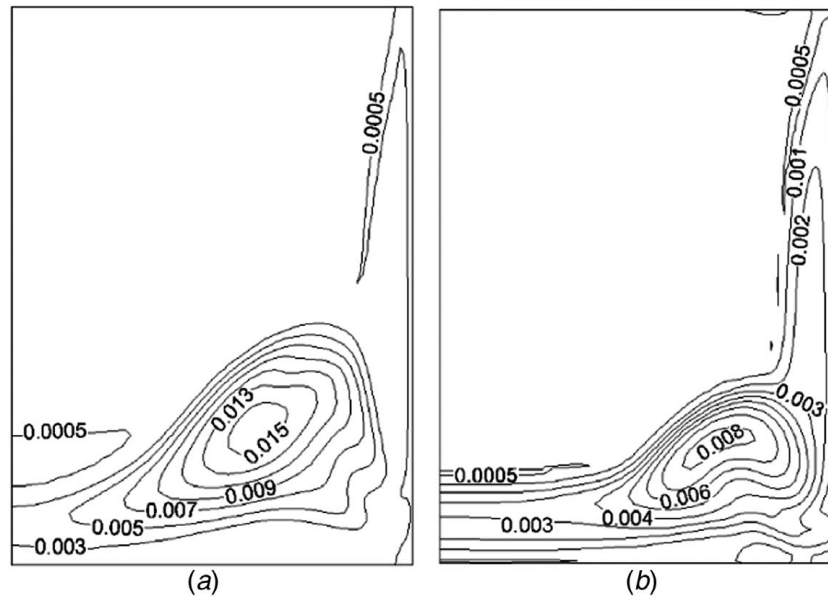


Fig. 16 Turbulent viscosity at 50% axial chord downstream, at an incidence angle of 0 deg: (a) SST and (b) SST-helicity

the corner separation region in compressors. The SST-helicity model is tested in the PVD cascade under two incoming flow conditions. The CPU cost of the SST-helicity model is almost the same as the original SST model, and the convergence of the SST-helicity model is better. The helicity modification suppressed the unrealistic corner separation extent and prevented premature corner stall. The SST-helicity model was shown to significantly improve predictive accuracy for the corner separation. A better agreement with the experimental measurements was obtained for the endwall streamlines, surface static pressure coefficient distributions, total pressure loss coefficient magnitude, and the corner separation extent. The SST-helicity model, therefore, offers promise for practical engineering application of compressor flows.

Finally, detailed turbulence quantities are analyzed to reveal the underlying flow physics. The SST-helicity model reduces the turbulence viscosity in the corner separation, which is consistent with the turbulence theory based on helicity analysis. Furthermore, supplementary comparisons are made against the solution from the RSM. The production of turbulent kinetic energy P_k (or P_{kh}), the

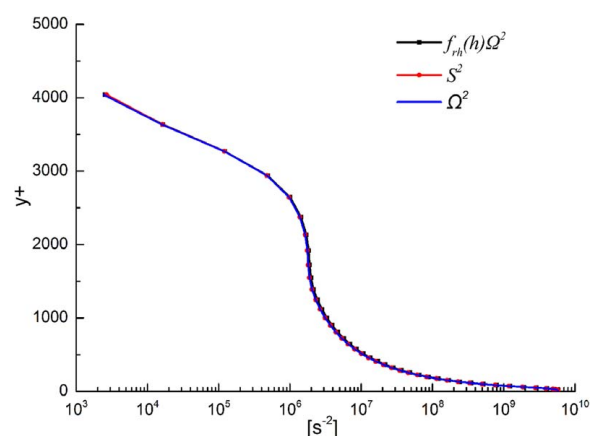
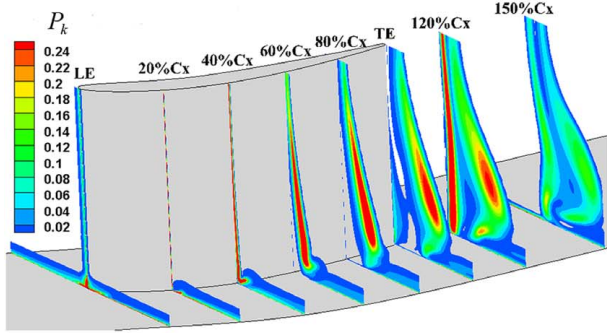
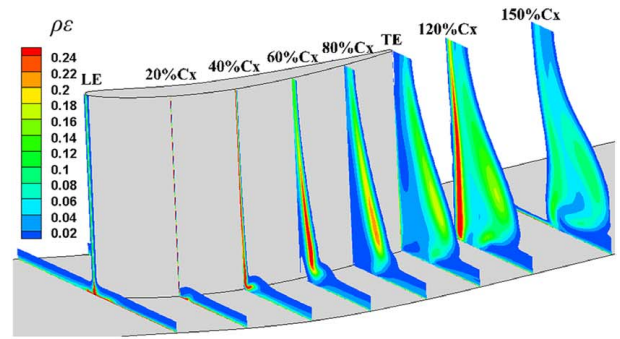


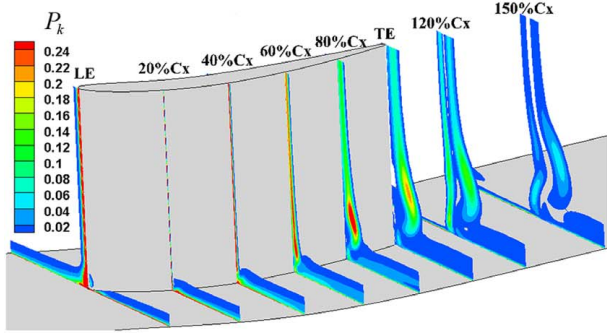
Fig. 17 Spanwise distribution of $f_{rh}(h)\Omega^2$, S^2 , Ω^2 in the $50\%C_x$ ahead of the leading edge



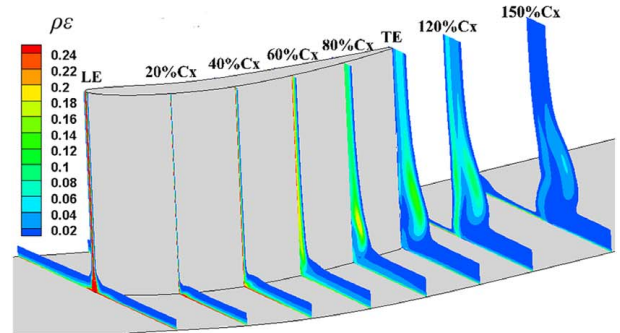
(a)



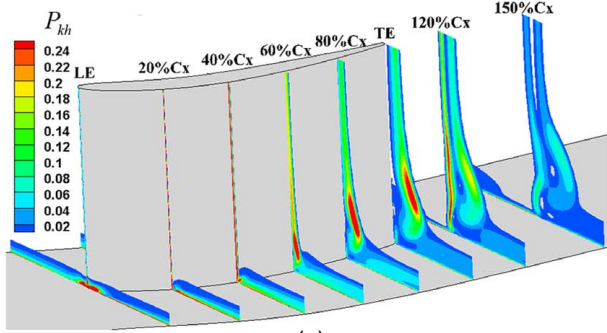
(a)



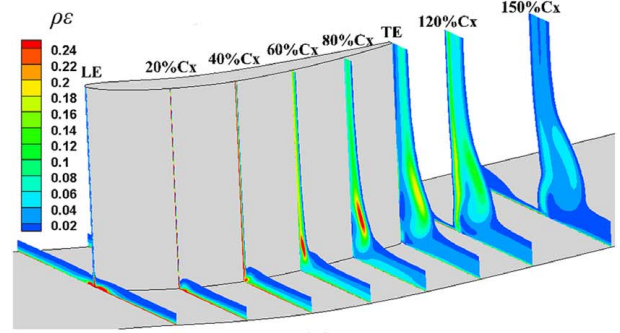
(b)



(b)



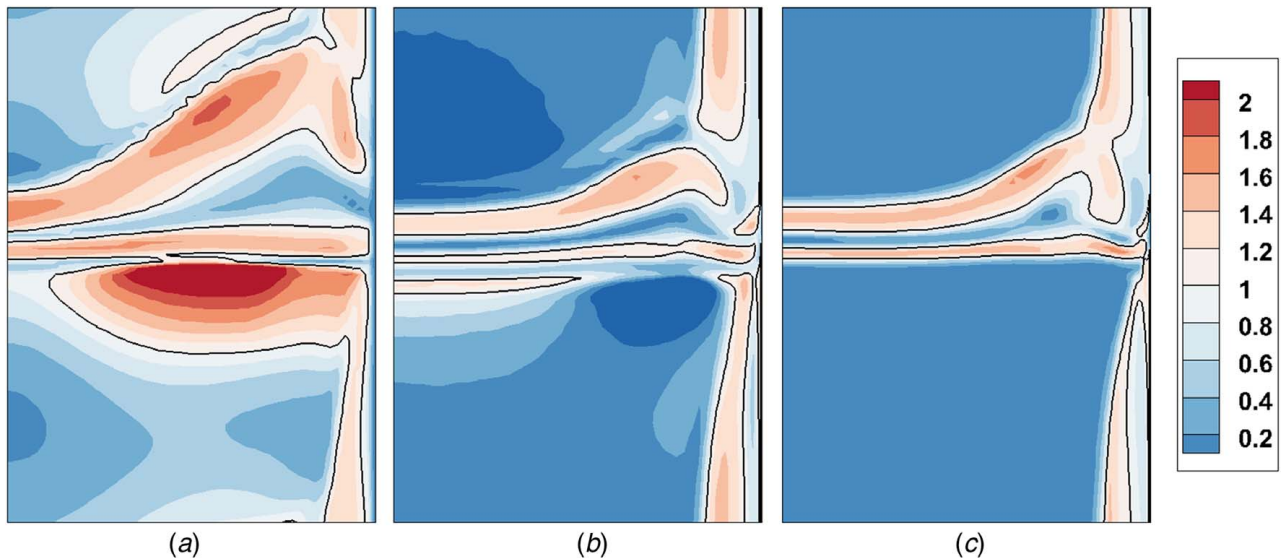
(c)



(c)

Fig. 18 Production of k in different flow stream surface under the incidence angle of 0 deg: (a) SST, (b) RSM_LPS, and (c) SST-helicity

Fig. 19 Turbulence dissipation rate $\rho\epsilon$ in different flow stream surface under the incidence angle of 0 deg: (a) SST, (b) RSM_LPS, and (c) SST-helicity



(a)

(b)

(c)

Fig. 20 Ratio of production of turbulent kinetic energy P_k (or P_{kh}) to the turbulence dissipation rate $\rho\epsilon$ at 20% axial chord downstream under the incidence angle of 0 deg: (a) SST, (b) RSM_LPS, and (c) SST-helicity

turbulence dissipation rate $\rho\varepsilon$, and the ratio of P_k (or P_{kh}) to $\rho\varepsilon$ from the SST-helicity model are compared with the RSM and the original SST model's predictions. The comparison shows that the SST-helicity can predict the turbulence quantities well, whereas the original SST has large discrepancies compared with the RSM. To conclude, in terms of accuracy, the proposed SST-helicity model significantly improves the original SST model and is quite competitive with the RSM. In terms of the robustness and computational cost, the SST-helicity model is superior to the RSM.

Acknowledgment

We express our appreciation to the late Professor Lipeng Lu, whose contribution to this work was of great significance. This work is supported by the National Natural Science Foundation of China (Grant Nos. 51676007, 51420105008, 51976006, and 51790513). Yangwei Liu is supported by the China Scholarship Council (CSC) for a one-year visit to the University of Cambridge.

Nomenclature

c = chord
 h = normalized helicity
 k = turbulence kinetic energy
 p = pressure
 v = velocity
 x = spanwise location
 y = distance to the next surface
 S = modulus of the mean rate-of-strain tensor
 p_0 = total pressure
 C_p = static pressure coefficient
 C_x = axial chord length
 D_ω = cross-diffusion term
 P_k = production of k
 P_ω = production of ω
 Y_k = dissipation of k
 Y_p = total pressure loss coefficient
 Y_ω = dissipation of ω
 y^+ = dimensional wall distance
 Γ_k = effective diffusivity of k
 Γ_ω = effective diffusivity of ω
 δ_{eff}^* = relative displacement thickness
 ρ = density
 ε = turbulence dissipation rate
 μ_t = turbulence viscosity
 ω = specific dissipation rate
 ω = vorticity vector
 Ω = modulus of the mean rate-of-vorticity tensor

References

- Lei, V. M., Spakovszky, Z. S., and Greitzer, E. M., 2008, "A Criterion for Axial Compressor Hub-Corner Stall," *ASME J. Turbomach.*, **130**(3), p. 031006.
- Denton, J. D., 1993, "Loss Mechanisms in Turbomachines," *ASME J. Turbomach.*, **115**(4), pp. 621–656.
- Gbadebo, S. A., Hynes, T. P., and Cumpsty, N. A., 2004, "Influence of Surface Roughness on Three-Dimensional Separation in Axial Compressors," *ASME J. Turbomach.*, **126**(4), pp. 455–463.
- Gbadebo, S. A., Cumpsty, N. A., and Hynes, T. P., 2005, "Three-Dimensional Separations in Axial Compressors," *ASME J. Turbomach.*, **127**(2), pp. 331–339.
- Courtiade, N., and Ottavy, X., 2013, "Experimental Study of Surge Precursors in a High-Speed Multistage Compressor," *ASME J. Turbomach.*, **135**(6), p. 061018.
- Liu, Y. W., Yan, H., and Lu, L. P., 2016, "Numerical Study of the Effect of Secondary Vortex on Three-Dimensional Corner Separation in a Compressor Cascade," *Int. J. Turbo Jet Eng.*, **33**(1), pp. 9–18.
- Liu, Y. W., Lu, L. P., Fang, L., and Gao, F., 2011, "Modification of Spalart-Allmaras Model With Consideration of Turbulence Energy Backscatter Using Velocity Helicity," *Phys. Lett. A*, **375**(24), pp. 2377–2381.
- Scillitoe, A. D., Tucker, P. G., and Adami, P., 2015, "Evaluation of RANS and ZDES Methods for the Prediction of Three-Dimensional Separation in Axial Flow Compressors," *ASME Paper No. GT2015-43975*.
- Liu, Y. W., Yan, H., Fang, L., Lu, L. P., Li, Q. S., and Shao, L., 2016, "Modified $k-\omega$ Model Using Kinematic Vorticity for Corner Separation in Compressor Cascade," *Sci. China Technol. Sci.*, **59**(5), pp. 795–806.
- Liu, Y. W., Yan, H., Liu, Y. J., Lu, L. P., and Li, Q. S., 2016, "Numerical Study of Corner Separation in a Linear Compressor Cascade Using Various Turbulence Models," *Chin. J. Aeronaut.*, **29**(3), pp. 639–652.
- Gbadebo, S. A., Cumpsty, N. A., and Hynes, T. P., 2008, "Control of Three-Dimensional Separations in Axial Compressor by Tailored Boundary Layer Suction," *ASME J. Turbomach.*, **130**(1), p. 011004.
- Evans, S., Hodson, H., Hynes, T., and Wakelam, C., 2010, "Flow Control in a Compressor Cascade at High Incidence," *AIAA J. Propul. Power*, **26**(4), pp. 828–836.
- Liu, Y. W., Sun, J. J., and Lu, L. P., 2014, "Corner Separation Control by Boundary Layer Suction Applied to a Highly Loaded Axial Compressor Cascade," *Energies*, **7**(12), pp. 7994–8007.
- Staats, M., and Nitsche, W., 2016, "Active Control of the Corner Separation on a Highly Loaded Compressor Cascade With Periodic Nonsteady Boundary Conditions by Means of Fluidic Actuators," *ASME J. Turbomach.*, **138**(3), p. 031004.
- Liu, Y. W., Sun, J. J., Tang, Y. M., and Lu, L. P., 2016, "Effect of Slot at Blade Root on Compressor Cascade Performance Under Different Aerodynamic Parameters," *Appl. Sci.*, **6**(12), p. 421.
- Denton, J. D., 2010, "Some Limitations of Turbomachinery CFD," *ASME Paper No. GT2010-22540*.
- Yan, H., Liu, Y. W., Li, Q. S., and Lu, L. P., 2018, "Turbulence Characteristics in Corner Separation in a Highly Loaded Linear Compressor Cascade," *Aerosp. Sci. Technol.*, **75**, pp. 139–154.
- Scillitoe, A. D., Tucker, P. G., and Adami, P., 2017, "Numerical Investigation of Three-Dimensional Separation in an Axial Flow Compressor: the Influence of Freestream Turbulence Intensity and Endwall Boundary Layer State," *ASME J. Turbomach.*, **139**(2), p. 021011.
- Liu, Y. W., Yan, H., Lu, L. P., and Li, Q. S., 2017, "Investigation of Vortical Structures and Turbulence Characteristics in Corner Separation in a Linear Compressor Cascade Using DDES," *ASME J. Fluids Eng.*, **139**(2), p. 021107.
- Lin, D., Su, X. R., and Yuan, X., 2018, "DDES Analysis of the Wake Vortex Related Unsteadiness and Losses in the Environment of a High-Pressure Turbine Stage," *ASME J. Turbomach.*, **140**(4), p. 041001.
- Liu, Y. W., Zhong, L. Y., and Lu, L. P., 2019, "Comparison of DDES and URANS for Unsteady Tip Leakage Flow in an Axial Compressor Rotor," *ASME J. Fluids Eng.*, **141**(12), p. 121405.
- Spalart, P. R., 2012, *Progress in Hybrid RANS-LES Modelling*, Springer-Verlag, Berlin, pp. 7–24.
- Liu, Y. W., Tang, Y. M., Liu, B. J., and Lu, L. P., 2019, "An Exponential Decay Model for the Deterministic Correlations in Axial Compressors," *ASME J. Turbomach.*, **141**(2), p. 021005.
- Liu, Y. W., Yu, X. J., and Liu, B. J., 2008, "Turbulence Models Assessment for Large-Scale Tip Vortices in an Axial Compressor Rotor," *AIAA J. Propul. Power*, **24**(1), pp. 15–25.
- Dunham, J., 1998, "CFD Validation for Propulsion System Components," *AGARD-AR-355*.
- Xie, Z., Liu, Y. W., Liu, X. H., Lu, L. P., and Sun, X. F., 2019, "Effect of RANS Method on the Stall Onset Prediction by an Eigenvalue Approach," *ASME J. Fluids Eng.*, **141**(3), p. 031401.
- Ma, L., Lu, L. P., Fang, J., and Wang, Q. H., 2014, "A Study on Turbulence Transportation and Modification of Spalart-Allmaras Model for Shock-Wave/Turbulent Boundary Layer Interaction Flow," *Chin. J. Aeronaut.*, **27**(2), pp. 200–209.
- Liu, Y. W., Wu, J. N., and Lu, L. P., 2016, "Performance of Turbulence Models for Transonic Flows in a Diffuser," *Mod. Phys. Lett. B*, **30**(25), p. 1650326.
- Spalart, P. R., and Allmaras, S. R., 1994, "A One-Equation Turbulence Model for Aerodynamic Flows," *Recherche Aeronautique*, **1**(1), pp. 5–21.
- Spalart, P., and Shur, M., 1997, "On the Sensitization of Turbulence Models to Rotation and Curvature," *Aerosp. Sci. Technol.*, **1**(5), pp. 297–302.
- Spalart, P. R., 2000, "Strategies for Turbulence Modelling and Simulations," *Int. J. Heat Fluid Flow*, **21**(3), pp. 252–263.
- Rung, T., Bunge, U., Schatz, M., and Thiele, F., 2003, "Restatement of the Spalart-Allmaras Eddy-Viscosity Model in Strain-Adaptive Formulation," *AIAA J.*, **41**(7), pp. 1396–1399.
- Menter, F. R., Kuntz, M., and Langtry, R., 2003, "Ten Years of Industrial Experience with the SST Turbulence Model," *Turbul. Heat Mass Transfer*, **4**(4), pp. 625–632.
- Menter, F. R., 1994, "Two-equation Eddy-Viscosity Turbulence Models for Engineering Applications," *AIAA J.*, **32**(8), pp. 269–289.
- Smirnov, P. E., and Menter, F. R., 2009, "Sensitization of the SST Turbulence Model to Rotation and Curvature by Applying the Spalart-Shur Correction Term," *ASME J. Turbomach.*, **131**(4), p. 041010.
- Brissaud, A., Frisch, U., Legerat, J., and Lesieur, M., 1973, "Helicity Cascades in Fully Developed Isotropic Turbulence," *Phys. Fluids*, **16**(8), pp. 1366–1367.
- Kraichnan, R. H., 1973, "Helical Turbulence and Absolute Equilibrium," *J. Fluid Mech.*, **59**(4), pp. 745–752.

- [38] Biferale, L., Musacchio, S., and Toschi, F., 2012, "Inverse Energy Cascade in Three-Dimensional Isotropic Turbulence," *Phys. Rev. Lett.*, **108**(16), p. 164501.
- [39] Moffatt, H. K., 1969, "The Degree of Knottedness of Tangled Vortex Lines," *J. Fluid Mech.*, **35**(1), pp. 117–129.
- [40] Scheeler, M. W., Van Rees, W. M., Kedia, H., Kleckner, D., and Irvine W. T. M., 2017, "Complete Measurement of Helicity and its Dynamics in Vortex Tubes," *Science*, **367**(6350), pp. 487–491.
- [41] Moffatt, H. K., 2017, "Helicity-Invariant Even in a Viscous Fluid," *ASME J. Tribol.*, **357**(6350), pp. 448–449.
- [42] Belian, A., Chkhetiani, O., Golbraikh, E., and Moiseev, S., 1998, "Helical Turbulence: Turbulent Viscosity and Instability of the Second Moments," *Physica A*, **258**(1), pp. 55–68.
- [43] Tang, Y. M., Liu, Y. W., and Lu, L. P., 2018, "Solidity Effect on Corner Separation and Its Control in a High-Speed Low Aspect Ratio Compressor Cascade," *Int. J. Mech. Sci.*, **142**, pp. 304–321.
- [44] Lee, K. B., Wilson, M., and Vahdati, M., 2018, "Validation of a Numerical Model for Predicting Stalled Flows in a Low-Speed Fan-Part I: Modification of Spalart-Allmaras Turbulence Model," *ASME J. Turbomach.*, **140**(5), p. 051008.
- [45] Kim, S., Pullan, G., Hall, C. A., Grewe, R. P., Wilson, M. J., and Gunn, E., 2019, "Stall Inception in Low Pressure Ratio Fans," *ASME J. Turbomach.*, **141**(7), p. 071005.
- [46] Kato, M., and Launder, B. E., 1993, "The Modelling of Turbulent Flow Around Stationary and Vibrating Square Cylinders," Ninth Symposium on Turbulent Shear Flows, No. 10-4, Kyoto, Japan, Aug. 16–18.
- [47] Barth, T. J., and Jespersen, D., 1989, "The Design and Application of Upwind Schemes on Unstructured Meshes," AIAA 27th Aerospace Sciences Meeting, Reno, Nevada, Technical Report AIAA-89-0366.
- [48] Gbadebo, S. A., 2004, "Three-dimensional Separations in Compressors," Doctoral thesis, University of Cambridge, UK, <https://doi.org/10.17863/CAM.7010>
- [49] Gibson, M. M., and Launder, B. E., 1978, "Ground Effects on Pressure Fluctuations in the Atmospheric Boundary Layer," *J. Fluid Mech.*, **86**(3), pp. 491–511.
- [50] Ditlevson, P., and Guiliani, P., 2001, "Cascade in Helical Turbulence," *Phys. Rev. E*, **63**(3), p. 036314.
- [51] Tang, Y. M., Liu, Y. W., and Lu, L. P., 2019, "Evaluation of Compressor Blading with Blade End Slots and Full-Span Slots in a Highly Loaded Compressor Cascade," *ASME J. Turbomach.*, **141**(12), p. 121002.